ACS Energy LETTERS

http://pubs.acs.org/journal/aelccp

# Machine Learning a Million Cycles as 2D Images from Practical Batteries for Electric Vehicle Applications

Xi Chen, Jeesoon Choi,* and Xin Li*

Cite This: *ACS Energy Lett.* 2022, 7, 4362−4367

Read Online

ACCESS | Metrics & More | Article Recommendations | Supporting Information

**ABSTRACT:** **It is a common intuition from battery experts that many shape features in the voltage profile image contain abundant information related to battery performance. However, such features are often too subtle for a human to extract by eye inspection and further correlate with battery performance. Using long cycling data from hundreds of large-format pouch cells and a total of 2 million cycles tested over 1000 days, we demonstrate here for the first time that it is advantageous to accurately predict the capacity and remaining useful life in real time by learning battery voltage profile images rather than voltage values. A strategy of end-to-end performance prediction of large-format battery cells is thus demonstrated to be feasible using only a few of the previous cycles at any given time point during the cycling test. Our work paves the way toward the application of machine learning for real-time battery performance prediction and regulation for electric vehicle applications.**

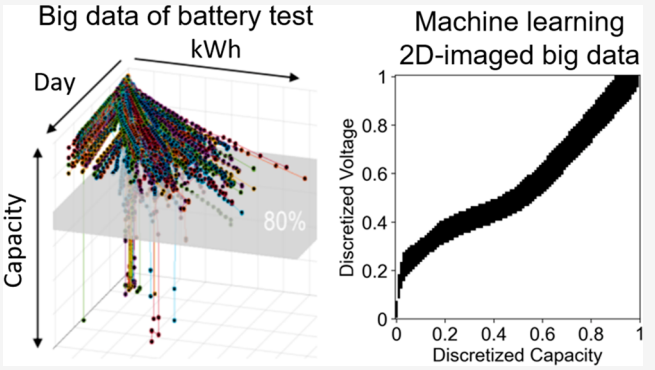


Li-ion batteries have made ever-increasing contributions to the switch to sustainable energy, the environment, and the climate in recent years, especially those used in electric vehicles (EVs). EVs are an important part of the current trend of global electrification. However, only 2% of cars on the road nowadays are EVs, while the remaining 98% are still gasoline cars. The slow electrification of cars is partly impeded by the performance, cost, and safety issues of batteries. A battery management system (BMS) is widely used to monitor real-time battery conditions. Thus, there have been great interest and effort in applying machine learning for battery performance monitoring, prediction, and safety[1−7] so that such a functionality can be more widely incorporated into the BMS in the future.

Machine learning has also been playing a more and more important role in facilitating battery development. On the material side, it has found success in the high-throughput screening of candidate materials for better battery performance.[8−11] On the practical side, it has also been demonstrated that machine learning models can effectively learn from battery testing data to forecast and evaluate battery performance and detect battery failure.[1,3,12] These methods not only save a considerable amount of testing time but also have great potential to enhance the safety of batteries. The application is especially attractive for batteries installed in EVs, with the goal of managing charging procedures and usage patterns for performance enhancement and predicting and preventing potential safety issues from a running battery in real time.

However, many of the current machine-learning studies of battery performance prediction fall short connecting the small-format coin cells tested under a specially designed lab condition with the large-format pouch, prismatic, or cylindrical cells, i.e., those used in EVs, which are tested under a more general and practical condition. Furthermore, the existing methods either require sophisticated measurements beyond the simple galvanostatic constant-current electrochemical measurement or are developed from a specially constructed set of measurements. These methods thus often result in a strong correlation with several predetermined factors, which largely limits the generalization to broader scenarios. These issues have impeded the application of machine learning methods for practical battery performance predictions.

**Received:** August 10, 2022
**Accepted:** November 7, 2022






https://doi.org/10.1021/acsenergylett.2c01817
*ACS Energy Lett.* 2022, 7, 4362−4367

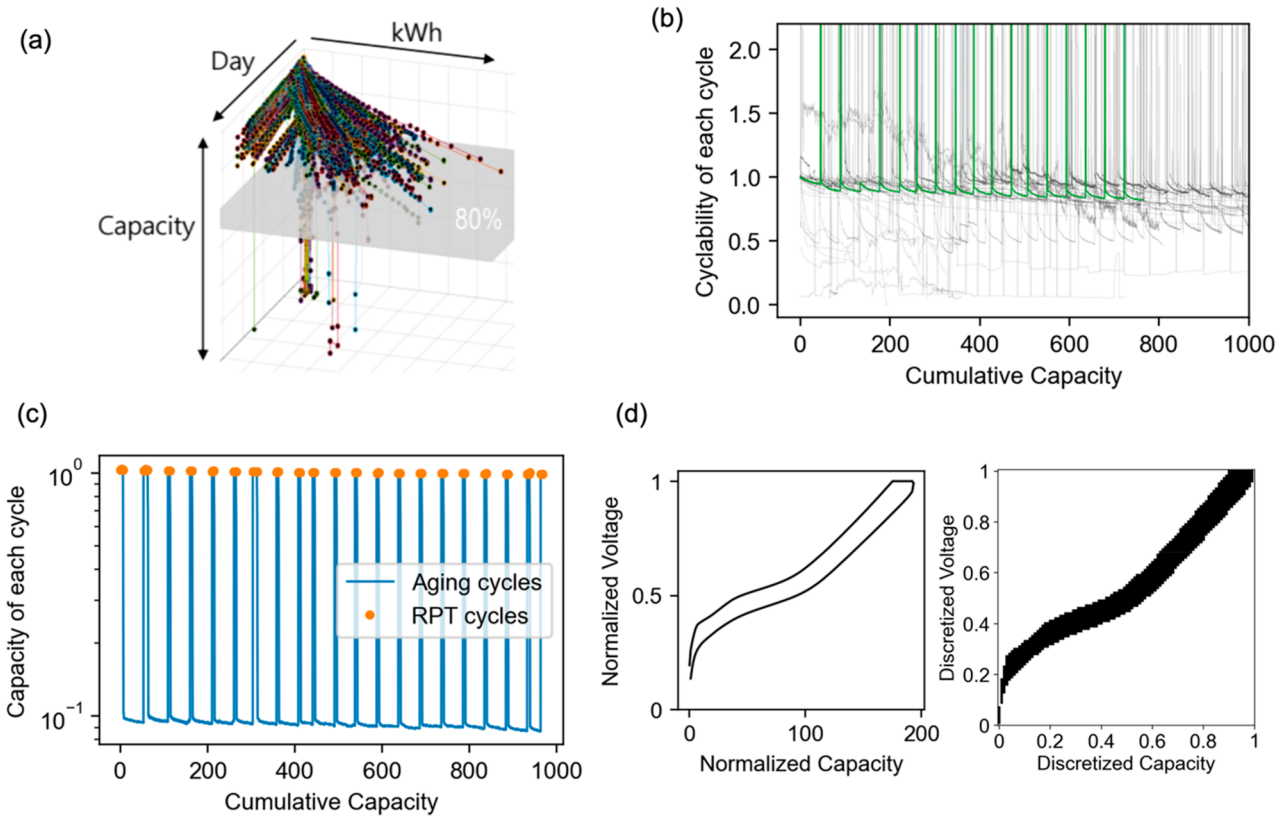


**Figure 1. (a) Global view of all data containing a total of 356 NMC−graphite pouch cell batteries with a capacity of 60 Ah monitored over 1000 days and 1000 kWh at various aging conditions, summing up to a total of 2 million aging cycles. (b) Normalized capacity ($Q$) versus normalized cumulative capacity for an example set of 50 batteries. The green curve highlights a particular battery test, where the spikes are from the RPT cycles and the remaining decay sections are the aging cycles that reflect capacity fading. (c) Illustration of actual aging and RPT periods for a particular battery test. (d) Illustration of our approach to representing the voltage profile of each cycle (left) using a binary image (right).**

In our previous study,[1] we introduced a method of treating battery cycling curves as 2D images to directly model their correlation with the target quantities. However, the method was developed based on coin cell data of short cycling tests around 30−50 cycles from the research laboratory. In this work, we developed an end-to-end approach for the first time for battery data from an industrial large-format pouch cell of 60 Ah capacity with long cycling tests that add up to a total of 2 million 2D images of cycles tested over 1000 days. To obtain better shape features of the cycling curves, we used the embeddings computed by pretrained foundational convolutional neural network models. Multiple factors are considered, including the shape features, the temperature, and the temperature fluctuation. We took advantage of the historical cycling data at any time point during the cycling test and achieved accurate modeling of two important and useful targets: the state of health (SOH) and the remaining useful life. We have demonstrated that the historical cycling information plays a critical role in forecasting the battery performance. Our result paves the way for the future application of machine learning-based battery performance prediction to the BMS systems of EVs and to the further understanding of battery (electro)chemistry evolutions.

LG Energy Solution collected the test cases from a total of 356 individual large-format 60 Ah pouch cells for EV battery application (Figure 1a). For each cell, this consisted of extended cycling test up to 27 000 cycles, and thus a total of 2 million aging cycles from 356 pouch cells with a capacity of 60 Ah were tested over 1000 days. Tests are performed at different temperatures, state of charge (SOC) ranges, and charge or discharge rates, making the data set a valuable platform to apply machine learning models to understand how complicated practical testing environment can affect battery performance. These cycles with different testing conditions will be referred to as the "aging cycles" (Figure 1b and c). For every battery tested, reference performance tests (RPTs) are conducted repeatedly at certain intervals of cycles to monitor the cell capacity and resistance under a standardized condition (25 °C and cycling rate of $C/3$). Cycles measuring the standard capacity will be referred to as the "RPT cycles" (Figure 1b and c).

One example battery testing case is shown in Figure 2 and SI Figure S1a. The results show the typical voltage curve shape of a $LiNi_xMn_yCo_zO_2$ (NMC) cathode paired with a graphite anode in a normalized voltage range (Figure 2). For this particular battery, the aging test was performed at a $2C$ rate (black), while the RPT cycles were performed at a $C/3$ rate (red). In addition, normalized currents, normalized capacity, and the actual testing temperatures are also presented in SI Figure S1b−d, respectively. For this particular battery, low-temperature cycling tests were performed around 10−17.5 °C, while the RPT tests were performed at room temperature around 25 °C. The small temperature fluctuations of the RPT tests are normal and are caused by the heat generated from the cycling of cells.



https://doi.org/10.1021/acsenergylett.2c01817
ACS Energy Lett. 2022, 7, 4362−4367

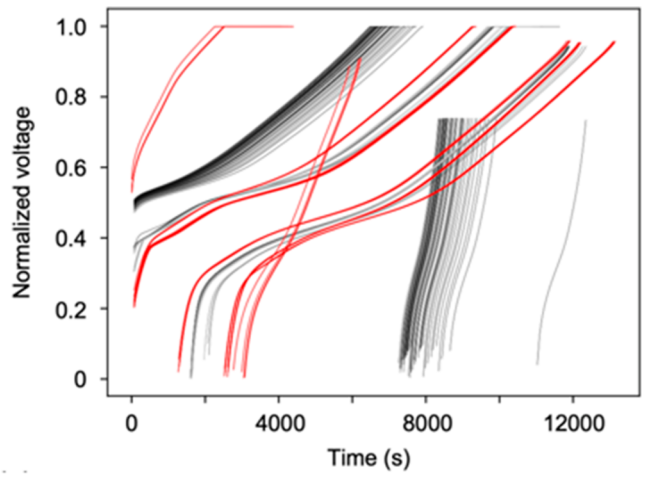


**Figure 2. Profile of normalized cycling voltage curves from an example battery tested for 1000 cycles. Darker curves correspond to later cycles. Red curves are from the reference performance tests (RPT).**

Beyond the measured electrochemical data, including the voltage profile and capacity, we identified the testing temperature as another important factor related to battery performance. As shown in Figure 3a, we visualized the battery temperature fluctuation at each cycle for each battery of the 356 pouch cell batteries. As shown in Figure 3b, we plotted the correlation between the temperature fluctuation at a given cycle and the capacity decreasing speed after this cycle. The overall correlation reaches 0.53, suggesting that temperature fluctuation has a nonnegligible influence on battery performance and can thus be integrated into the battery performance prediction.

In order to obtain the embedding features for these cycling curve images, or the cycling curve matrices, we take advantage of open-sourced foundational convolution neural network models (e.g., the Tensorflow[13] Hub). These are very deep convolutional neural networks trained on a benchmark natural image data set, ImageNet,[14] with more than 10 million images describing objects across 1000 classes. Studies have demonstrated that such foundation models possess general image-understanding capabilities ranging from astronomical images[15] to medical images,[16] and other industrial images.

As illustrated in Figure 4a, we performed feature extraction using a ResNet-50[17] model with 50 layers and obtained a

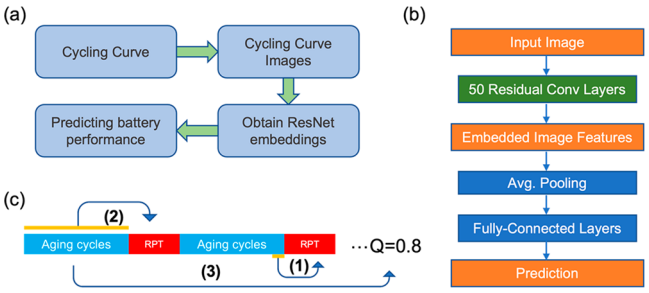


**Figure 4. (a) Schematic of obtaining embedding features of cycling curve images from ResNet and using them for performance prediction. (b) Diagram of a ResNet-50 model with 50 residual convolution layers.[17] The cycling curve images we prepared are used as "Input Image" to the model, and the output of the "Average Pooling" layer is taken as computed feature vector for our cycling curve image. (c) Illustration of the different forecast schemes studied, where three schemes are labeled as (1), (2), and (3) beside the three arrows. Scheme (1) is about using information from a single or several aging cycles to predict the capacity of the reference performance test, while scheme (2) uses several consecutive cycles in history. Scheme (3) is related to the prediction of the remaining useful life, i.e., the cumulative capacity before the RPT capacity drops below 80%.**

1000-dimensional embedding vector for each cycling curve image. Figure 4b shows a schematic diagram of the ResNet-50 model to which we feed the cycling curve images as the input images and then record the output vector from the second-to-last layer. Since the model has been well trained to recognize images, we reduce the cycling curve image to a 1000-dimensional vector, which not only condenses the information contained in the cycling curves but also enlarges the difference between different cycling curve images as much as possible. In order to make our model more scalable with a faster computational speed, we apply a principal component analysis, which reduces the dimension of the embedding feature vector from 1000 to 32 or 64 for later study. We will refer to these as

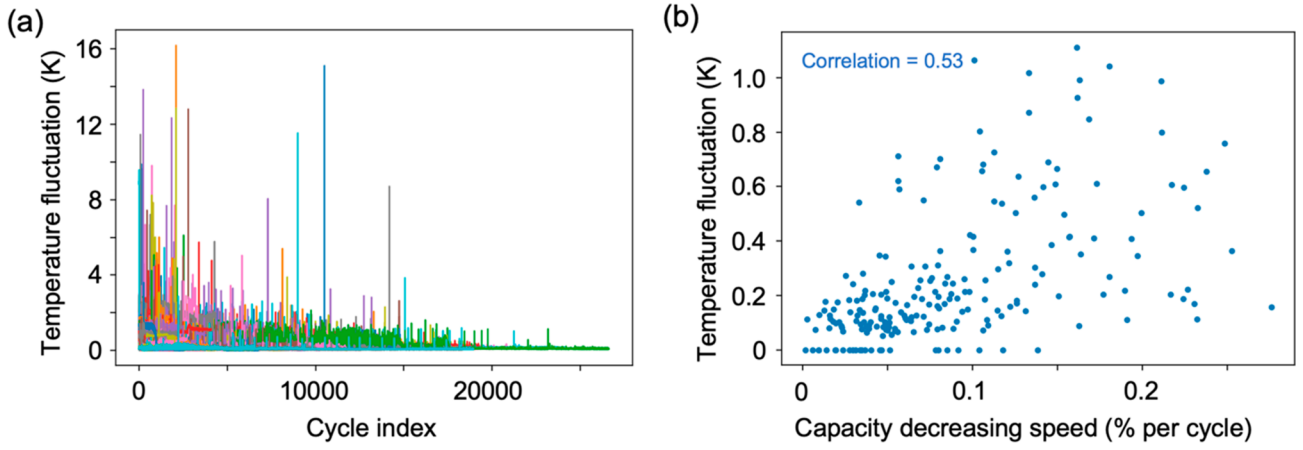


**Figure 3. Temperature fluctuation statistics for all batteries. (a) Temperature fluctuation for each cycle of every battery of the 356 pouch cell batteries. A different color was applied automatically for each cell. (b) Correlation between the temperature fluctuation in each cycle and the capacity decreasing speed after the corresponding cycle.**



https://doi.org/10.1021/acsenergylett.2c01817
ACS Energy Lett. 2022, 7, 4362−4367

the 32-dimensional and 64-dimensional shape features in the following sections.

Figure 4c shows the diagram of several possible prediction schemes related to capacity prediction. We considered various time spans of information used for the prediction, including using the immediate aging cycle before the RPT test or a few aging cycles before the RPT test. To construct the input−output pairs to model, we use the capacity of each of the RPT cycle from every battery as the target and use the information on the aging cycles before the RPT cycle to construct the input features. We start with only the shape features of the aging cycling curves and then combine them with the capacity (feature $Q$) and the mean and variance of temperature (feature $T$) of the aging cycles. We feed these features into a random forest as the regression model, which learns to output the correct value for the RPT capacity.

Figure 5a and b show the per-example training and testing result distribution using just 32 shape features of a single aging

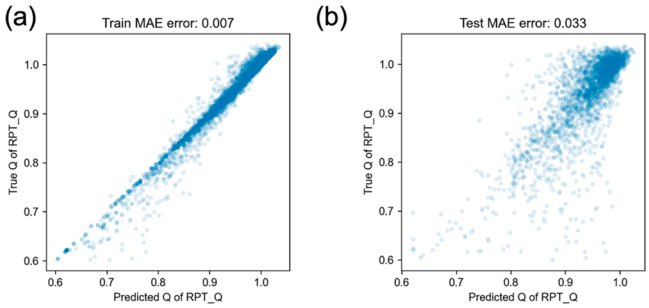


**Figure 5. (a) Per-example training and (b) test error of the RPT capacity prediction.**

cycle before the RPT cycle as the input, where the plotted ($x$, $y$) are (predicted value, true value). We see that using just 32 shape features can already achieve decent training accuracy, as indicated by the fact that the data points are well-aligned along the $y = x$ line. To further increase the generalization capability of our method, we tested a few different strategies. We find that simply adding more input features does not improve the learning result, as shown in the second row of Table 1, as the 64-dimensional shape features achieve the same result as 32-dimensional shape features. Instead, we find that using different types of information is helpful. As shown in the third and fourth rows of Table 1, we combined the shape feature with the capacity and temperature fluctuations of the aging cycles, respectively, and observed 10% reductions in both training and test errors.

**Table 1. Result of the RPT SOH Estimation Using Previous Aging Cycles[a]**

| input features | total feature length | training error | test error |
|---|---|---|---|
| 1 cycle | 32 | 0.007 | 0.033 |
| 1 cycle | 64 | 0.007 | 0.033 |
| 1 cycle | 33 (+Q) | 0.006 | 0.030 |
| 1 cycle | 35 (+Q + T) | 0.006 | **0.029** |
| 1 cycle only $Q$ | 1 | 0.012 | 0.058 |
| 1 cycle only $T$ | 2 | 0.012 | 0.053 |
| stacking 3 cycles | 105 (+Q + T) | 0.005 | 0.024 |
| stacking 10 cycles | 350 (+Q + T) | 0.005 | **0.025** |

[a]The input shape features have a dimension of either 32 or 64. $Q$ is the scalar value of the relative capacity, and $T$ is the temperature feature consisting of the mean and variance of the temperature of the corresponding cycle. "1 cycle" refers to using the information of the aging cycle right before the RPT test cycle, and "stacking 3 cycles" means concatenating the features from the last three aging cycles before the RPT test cycle.

As the battery performance is highly history-dependent, it turns out that the historical information can indeed provide critical ingredients to our modeling. For the 35-dimensional features of each cycle (32 for shape, 1 for capacity $Q$, and 2 for temperature $T$), we first considered stacking these features of three consecutive aging cycles together before the target RPT cycle, making a concatenated 105-dimensional feature. Going from one cycle to three cycles as the input, we observed another 20% reduction in both training and test errors (Table 1). Further increasing the number of cycles from 3 to 10 does not bring extra advantage, suggesting that the short-range historical correlation is already captured by the 3 aging cycles before the RPT cycle. We note that the lack of low-$Q$ samples in the data set, due to the high capacity and cyclability of these high-quality batteries, may cause additional spread in the low-$Q$ regime in the test data. A more complete data set with more low-$Q$ and medium-$Q$ samples will further reduce the overall spread and increase the prediction.

For another practically important quantity, the remaining useful life, we are concerned with how much of the capacity we can have in future cycles before the standard RPT capacity drops to below 80% of the initial RPT capacity. Since only a small fraction of batteries have RPT capacities below 80% in our data, we define the average decreasing rate $D$ of the capacity after a given cycle as an equivalent quantity to the remaining useful life

$$D = \frac{Q_c(\mathrm{RPT}) - Q_f(\mathrm{RPT})}{\sum_c^f Q(\mathrm{aging})}$$

where "c" and "f" in the summation stand for "current" and "final" RPT cycles, respectively. Similar to our previous modeling of the RPT capacity, for each battery, all RPT cycles with a sufficient number of previous aging cycles are constructed as an example, where the aging cycles are used as input and the average decreasing rate $D$ is used as the target. Then, we applied similar techniques compared to those for the RPT capacity prediction to model the average decreasing rate.

The results in Table S1 carry a message similar to that we obtained from modeling the RPT capacity. The best result is also obtained by combining the shape, capacity, and temperature features when averaging these features over a few of the previous aging cycles. In Figure S2, the per-example training and test result distributions are also similar to those from modeling the RPT capacity. Note that the error from modeling the remaining useful life is about three times larger than that from modeling the RPT capacity. This is caused by the fact that the distribution of the capacity decreasing rate is about three times wider than that of the RPT capacity. Thus, the relative error of modeling these two tasks should be close. The result suggests that our model and methodology is capable of both tasks, namely, predicting both capacity and remaining useful life with high accuracy given the right training dataset of batteries.

It is worth noting that these battery cycling data are in fact temporal sequences. Although ResNET itself does not contain temporal information, we included the temporal information both inside each cycle and across different cycles in our



https://doi.org/10.1021/acsenergylett.2c01817
ACS Energy Lett. 2022, 7, 4362−4367

algorithm. First, since we represent each cycling curve as images (e.g., Figure 1d), the temporal information within each cycle is modeled as spatial information that can be captured by the features produced from ResNET. For temporal information from cycle to cycle, we applied a straightforward method of stacking the features of consecutive cycles together, creating a temporal feature order for the model to learn. That said, it is worth trying in the future a recurrent neural network (RNN) or attention mechanisms that are also good at modeling sequences. Technically, we showed that averaging the features over some histories is the best approach for the prediction accuracy, emphasizing the importance of historical cycling information in forecasting the battery performance. Since the historical cycling information reflects the (electro)chemical evolution history, its correlation with the future capacity and remaining useful life reflects the general stability and predictable instability of electrochemical reactions in commercial large-format pouch cells. Our work paves the way toward the application of machine learning for real-time EV battery performance prediction and regulation in the future.

## METHODS

**Battery Cycling Data.** LG Energy Solution collected the test cases from a total of 356 individual large-format 60 Ah pouch cells for EV battery application. For each cell composed of a NMC cathode and a graphite anode, it consists of an extended cycling test up to 27000 cycles; thus, there are a total of several million cycles in the dataset. The data were collected over 1000 days and 1000 kWh at various aging conditions. More details can be found in the main text regarding Figure 1 and Figure 2.

**Machine Learning.** Following previous literature,[1] we prepared each test cycle (see Figure 1d) as a 224 × 224 binary image matching the standard resolution of ResNet. The region between the charge and discharge curve is given the value 1, and the rest is given the value 0. The Resnet model we used to compute embedding features for the cycling curve images was constructed through the Keras[18] Applications API, with model parameters pretrained on ImageNet as described previously.[17]

We use decision trees to perform the regression modeling mainly due to their robustness. A decision tree starts with the $n$ input features $\{x_1, x_2, ..., x_n\}$, where each node of the tree applies a conditional statement on the value of a feature, moving to a subsequent node based on the truth of that statement. The optimization of the tree includes choosing both the feature and the threshold for the criteria for each node that overall best split the set of items. Instead of measuring the error, better metrics such as the cross entropy and the Gini index are generally used to measure the goodness of the choice of the criteria and the data split.[8,19] We use an ensemble model of individual decision trees, the extremely randomized tree model.[20] In such models, a number of $N$ trees are initialized simultaneously ($N$ = 30 in our setting). Each tree in the ensemble is fed with training data sampled from the training set. A random subset of candidate features is used from which thresholds are drawn at random for each candidate feature, and the best of these randomly generated thresholds is picked as the splitting rule.

## ASSOCIATED CONTENT

### Supporting Information

The Supporting Information is available free of charge at https://pubs.acs.org/doi/10.1021/acsenergylett.2c01817.

Battery voltage curve, current, capacity, and temperature profiles of a battery with 1000 cycles; prediction result of the capacity decreasing rate or remaining useful life (RUL); and training and testing results of the capacity decreasing rate (PDF)

## AUTHOR INFORMATION


### Corresponding Authors

**Xin Li** − *John A. Paulson School of Engineering and Applied Sciences, Harvard University, Cambridge, Massachusetts 02138, United States;* orcid.org/0000-0001-9390-0830; Email: lixin@seas.harvard.edu

**Jeesoon Choi** − *BMS AI Development Team, LG Energy Solution, Seoul 07335, Republic of Korea;* Email: jeesoonchoi@lgensol.com

### Author

**Xi Chen** − *John A. Paulson School of Engineering and Applied Sciences, Harvard University, Cambridge, Massachusetts 02138, United States;* orcid.org/0000-0002-1581-4627

Complete contact information is available at: https://pubs.acs.org/10.1021/acsenergylett.2c01817


### Notes

The authors declare no competing financial interest.

## ACKNOWLEDGMENTS

This work is supported by the Global Innovation Contest (GIC) of LG Energy Solution, Ltd.; a Data Science Initiative Competitive Research Award at Harvard University; and the Climate Change Solutions Fund at Harvard University.

## REFERENCES


(1) Chen, X.; Ye, L.; Wang, Y.; Li, X. Beyond-Expert-Level Performance Prediction for Rechargeable Batteries by Unsupervised Machine Learning. *Adv. Intell. Syst.* **2019**, *1*, 1900102.

(2) Aykol, M.; Herring, P.; Anapolsky, A. Machine Learning for Continuous Innovation in Battery Technologies. *Nat. Rev. Mater.* **2020**, *5*, 725.

(3) Lv, C.; et al. Machine Learning: An Advanced Platform for Materials Development and State Prediction in Lithium-Ion Batteries. *Adv. Mater.* **2022**, *34*, 2101474.

(4) Aykol, M.; et al. Perspective-Combining Physics and Machine Learning to Predict Battery Lifetime. *J. Electrochem. Soc.* **2021**, *168*, No. 030525.

(5) Severson, K. A.; et al. Data-Driven Prediction of Battery Cycle Life before Capacity Degradation. *Nat. Energy* **2019**, *4*, 383−391.

(6) Jiang, Z.; Li, J.; Yang, Y.; Mu, L.; Wei, C.; Yu, X.; Pianetta, P.; Zhao, K.; Cloetens, P.; Lin, F.; Liu, Y.; et al. Machine-Learning-Revealed Statistics of the Particle-Carbon/Binder Detachment in Lithium-Ion Battery Cathodes. *Nat. Commun.* **2020**, *11*, 2310.

(7) Lu, J.; Xiong, R.; Tian, J.; Wang, C.; Hsu, C. W.; Tsou, N. T.; Sun, F.; Li, J. Battery Degradation Prediction against Uncertain Future Conditions with Recurrent Neural Network Enabled Deep Learning. *Energy Storage Materials* **2022**, *50*, 139.

(8) Fitzhugh, W.; Chen, X.; Wang, Y.; Ye, L.; Li, X. Solid-Electrolyte-Interphase Design in Constrained Ensemble for Solid-State Batteries. *Energy & Environ. Sci.* **2021**, *14*, 4574.

(9) Wang, Y.; Ye, L.; Chen, X.; Li, X. A Two-Parameter Space to Tune Solid Electrolytes for Lithium Dendrite Constriction. *JACS Au* **2022**, *2*, 886.

(10) Moses, I. A.; Joshi, R. P.; Ozdemir, B.; Kumar, N.; Eickholt, J.; Barone, V. Machine Learning Screening of Metal-Ion Battery Electrode Materials. *ACS Appl. Mater. Interfaces* **2021**, *13*, 53355.

(11) Liu, Y.; Esan, O. C.; Pan, Z.; An, L. Machine Learning for Advanced Energy Materials. *Energy and AI* **2021**, *3*, 100049.
(12) Samanta, A.; Chowdhuri, S.; Williamson, S. S. Machine Learning-Based Data-Driven Fault Detection/Diagnosis of Lithium-Ion Battery: A Critical Review. *Electronics* **2021**, *10*, 1309.
(13) Abadi, M.; Agarwal, A.; Barham, P.; Brevdo, E.; Chen, Z.; Citro, C.; Corrado, G. S.; Davis, A.; Dean, J.; Devin, M.et al., TensorFlow: Large-Scale Machine Learning on Heterogeneous Distributed Systems; TensorFlow, 2015. Software available from https://www.tensorflow.org/.
(14) Deng, J.; Dong, W.; Socher, R.; Li, L.-J.; Li, K.; Fei-Fei, Li ImageNet: A Large-Scale Hierarchical Image Database. *2009 IEEE Conference on Computer Vision and Pattern Recognition* **2009**, 248−255.
(15) George, D.; Shen, H.; Huerta, E. A. Classification and Unsupervised Clustering of LIGO Data with Deep Transfer Learning. *Physical Review D* **2018**, *97*, 101501.
(16) Raghu, M.; Zhang, C.; Kleinberg, J.; Bengio, S.Transfusion: Understanding Transfer Learning for Medical Imaging. In *Proceedings of the 33rd International Conference on Neural Information Processing Systems*, Vancouver, Canada, December 8−14, 2019; NeurIPS, 2019; no. 301.
(17) He, K.; Zhang, X.; Ren, S.; Sun, J. Deep Residual Learning for Image Recognition. *2016 IEEE Conference on Computer Vision and Pattern Recognition (CVPR)* **2016**, 770−778.
(18) Chollet, F.et al.*Keras*; Keras, 2015. https://keras.io/ (accessed 2020-06-01).
(19) Bishop, C. M.*Pattern Recognition and Machine Learning*; Springer, 2006.
(20) Geurts, P.; Ernst, D.; Wehenkel, L. Extremely Randomized Trees. *Machine Learning* **2006**, *63*, 3.



https://doi.org/10.1021/acsenergylett.2c01817
*ACS Energy Lett.* 2022, 7, 4362−4367